Physics of the Earth and Planetary Interiors, 53 (1989) 432–443
Elsevier Science Publishers B.V., Amsterdam – Printed in The Netherlands

A moving finite element method for magnetotelluric modeling

Bryan J. Travis

Earth and Space Sciences Division, Los Alamos National Laboratory, Los Alamos, NM 87545 (U.S.A.)

Alan D. Chave *

Institute of Geophysics and Planetary Physics, University of California at San Diego, La Jolla, CA 92093 (U.S.A.)

(Received January 29, 1987; revision accepted August 20, 1987)

Travis, B.J. and Chave, A.D., 1989. A moving finite element method for magnetotelluric modeling. Phys. Earth Planet. Inter., 53: 432–443.

Finite element simulation of the electromagnetic fields in complex geological media is commonly used in interpreting field data. In this paper, recent, major improvements to finite element methodology are outlined. The implementation of a moving finite element technique, in which the mesh nodes are allowed to move adaptively to achieve an accurate solution, is described. Efficient matrix solutions based on incomplete factorization and matrix ordering are also discussed; these offer order of magnitude reductions in memory requirements and increases in execution speed. Finally, the advantages of adapting finite element codes to modern supercomputers are emphasized. These topics are illustrated by formulating a moving finite element forward model for the two-dimensional magnetotelluric problem. The result is validated by comparison with standard control models. While preliminary in nature, the result does indicate that substantial improvements to geophysical modeling can be achieved through the use of modern approaches.

1. Introduction

The experimental state-of-the-art in electromagnetic geophysics is currently in a condition of rapid evolution. This is owing in large part to the digital revolution, which has made reliable, portable instrumentation widely available and increased the utility of advanced data-processing methods, even in the field. However, the capability to model and interpret data in terms of electrical or geologic structure has lagged behind. This poses the single largest obstacle to the further development and wider application of electromagnetic principles in geophysics.

The finite element (FE) method, among several others, has received increasing attention in recent years for the numerical simulation of EM problems. Examples include the use of FE to model magnetotelluric (MT) fields in 2-D structures (Coggon, 1971; Lee and Morrison, 1985; Rodi, 1976; Wannamaker et al., 1987), and standard computer codes for this purpose are becoming available (e.g., Wannamaker et al., 1985). However, FE modeling with either more complex (i.e., controlled) sources or 3-D structures has not proven as satisfactory to date (e.g., Pridmore et al., 1981), and other approaches, especially integral equation methods, are in more general use. The advantages of the FE method include flexibility and a capability to handle complex structures in a straightforward manner. The principal disadvantage is the need for relatively extensive computing resources, especially storage. This has made FE somewhat difficult to implement on small computers.

* Present address: AT&T Bell Laboratories, 600 Mountain Ave., Murray Hill, NJ 07974, U.S.A.

Major improvements to 2-D and 3-D electromagnetic modeling codes can be made by incorporating recent advances in FE methodology and numerical algorithms which take full advantage of the structure inherent in FE matrices. First, the moving finite element (MFE) method incorporates adaptively moving nodes into the FE equations, substantially increasing the accuracy that is obtainable with a given size mesh. Second, while most MT modeling codes use Gaussian elimination or LU decomposition to solve the resulting matrix equations, considerably more efficient methods based on incomplete factorization (Behie and Forsyth, 1984) are now available. This approach results in an order of magnitude reduction in memory requirements, as well as a large increase in execution speed. Finally, while these tools will yield markedly better performance on conventional, scalar computers, the vector architecture of modern Class VI or VII supercomputers can yield additional speed improvements of up to a factor of several hundred with properly designed algorithms.

In this paper, the formulation of a 2-D MFE forward code for MT modeling is described. The emphasis is placed both on the MFE formalism and its implementation using modern numerical techniques. The code is validated by comparison to standard control models proposed by Weaver et al. (1985, 1986). This result is considered as an intermediate one by the authors, and can be improved by using more sophisticated basis functions, triangular elements, and similar enhancements. Ultimately, MFE will be used both in the development of a regularized inversion method for 2-D MT data and as a step toward a fully 3-D modeling code.

2. Governing equations

The physics of electromagnetic induction is described by the Maxwell equations in the quasi-static or pre-Maxwell limit, in which the magnetic effect of displacement current is neglected

$$\nabla \cdot \mathbf{B} = 0 \tag{1}$$

$$\nabla \times \mathbf{E} + \partial_t \mathbf{B} = 0 \tag{2}$$

$$\nabla \times (\mathbf{B}/\mu) - \sigma \mathbf{E} = 0 \tag{3}$$

where the symbols have their usual meaning. The role of electric charge in (1)–(3) is often confused. By removing the displacement current to give (3), phenomena with time-scales shorter than that of EM diffusion are filtered out, and charge appears to travel instantaneously. Electric charge is still present, usually in association with conductivity gradients or discontinuities, and its fields are quite important. This is especially true in 2-D and 3-D structures, and charge accounts for many of the important differences between simple 1-D and higher-dimensional realizations.

For a 2-D structure in which σ and μ are independent of the $\hat{x}$ co-ordinate, it is well known that the electromagnetic fields separate into two independent modes if the sources are also free of $\hat{x}$ dependence. The first of these is called the E-polarization or transverse electric (TE) mode, and is completely described by the field components E_x, B_y, and B_z. The second case is called the B-polarization or transverse magnetic (TM) mode, and involves only the B_x, E_y, and E_z fields. Following Rodi (1976), and assuming $e^{-i\omega t}$ dependence for all variables, the vector Maxwell equations (1)–(3) reduce to the generic scalar set

$$\partial_y I + \partial_z J + \gamma V = 0 \tag{4}$$

$$\partial_z V + \eta J = 0 \tag{5}$$

$$\partial_y V + \eta I = 0 \tag{6}$$

which may be combined to give the second-order partial differential equation

$$\partial_y(\partial_y V/\eta) + \partial_z(\partial_z V/\eta) - \gamma V = 0 \tag{7}$$

where the variables for the two modes are

	TM	TE
V	B_x/μ	E_x
J	$-E_y$	B_y/μ
I	E_z	$-B_z/\mu$
η	σ	$-i\omega\mu$
γ	$-i\omega\mu$	σ

At horizontal contacts between media of different conductivity or permeability, the quantities V, $\partial_z V/\eta$, and $\partial_y V$ are continuous, while at vertical contacts, V, $\partial_z V$, and $\partial_y V/\eta$ are continuous. EM induction in a 2-D medium is governed by two independent scalar equations for the principal

fields E_x and B_x. The auxiliary fields E_y, E_z, B_y, and B_z are obtained from (5) and (6). Note also that the TE mode involves an electric field which is always parallel to changes in the conductivity, and hence involves no electric charge. This is manifest in the absence of terms involving the conductivity gradient in the TE form of (7). By contrast, boundary charge is important in determining the behavior of the TM mode electric field. The eqns. (4)–(7) may be simplified for most real Earth problems by taking μ as constant and equal to the free space value; this will be assumed for all of the results in this paper.

3. MFE Solution

The resolution with which (7) can be solved depends strongly on the numerical methodology that is applied. For a given simulation, there are two basic ways to enhance performance. First, more accuracy can be achieved with a limited number of mesh nodes. Second, the computer usage and memory requirements can be minimized by taking advantage of the structure of the FE equations; this is discussed in the next section. Since most FE formulations use piecewise continuous linear basis functions between fixed nodes, one way to improve the accuracy is to use a higher order (e.g., quadratic) approximation in the discretization. This invariably leads to more complicated FE equations and a larger bandwidth for the FE matrices, and usually results in substantially longer computer run-times. A better approach involves an adaptive mesh, in which the nodes are allowed to move such that their locations actually become a part of the solution. The nodes will concentrate in regions of strong gradients where they are needed for good resolution. An attractive feature of this method is that low-order basis functions may be used without a significant loss in accuracy. An analogy can be made to two common methods for the numerical solution of ordinary differential equations. The standard Runge–Kutta method is not adaptive, and the order and step size must be chosen a priori to yield an adequate solution in the most complex part of solution space. This is similar to fixed mesh FE, where the node spacing must be chosen ahead of time to yield the required accuracy throughout the solution region. More modern predictor–corrector algorithms are far more efficient, varying the step size and order locally to achieve an accurate solution without using excessive computer time. This is analogous to MFE, and can handle more complicated equations in an automatic fashion with a substantial reduction in computer run-time. The MFE method was introduced by Miller (1981) and Miller and Miller (1981). Further developments and some illustrations of its operation are contained in Gelinas et al. (1981) and Dukowicz (1984).

The representation used in the present MFE formulation is a standard linear finite element type. The computational mesh is divided into rectangular cells with horizontal or vertical sides. The field values are specified at the centers of the zones. A linear element is defined for each quadrant of a zone. Denoting the indices of the zone by i, j, where i is the z-index and j is the y-index, yields the basic function

$$V = V_{ij} + a_{ij}^n (y - y_{j-1/2}) - b_{ij}^n (z - z_{i-1/2}) \qquad (8)$$

where the coefficients are

$$a_{ij}^1 = \frac{2\eta_{ij}(V_{ij} - V_{i,j-1})}{(\eta_{ij}\,\Delta y_j + \eta_{i,j-1}\,\Delta y_{j-1})}$$

$$a_{ij}^2 = \frac{2\eta_{ij}(V_{i,j+1} - V_{ij})}{(\eta_{ij}\,\Delta y_j + \eta_{i,j+1}\,\Delta y_{j+1})}$$

$$b_{ij}^1 = \frac{2\eta_{ij}(V_{i-1,j} - V_{ij})}{(\eta_{ij}\,\Delta z_i + \eta_{i-1,j}\,\Delta z_{i-1})}$$

$$b_{ij}^3 = \frac{2\eta_{ij}(V_{ij} - V_{i+1,j})}{(\eta_{ij}\,\Delta z_i + \eta_{i+1,j}\,\Delta z_{i+1})}$$

with $a_{ij}^3 = a_{ij}^1$, $a_{ij}^4 = a_{ij}^2$, $b_{ij}^2 = b_{ij}^1$, $b_{ij}^4 = b_{ij}^3$, $\Delta y_j \equiv y_j - y_{j-1}$, and $\Delta z_i \equiv z_i - z_{i-1}$. The cell quadrant indices n of 1–4 correspond to the upper left, upper right, lower left, and lower right corners; the co-ordinates of the lower right cell corner are (y_j, z_i); and the cell centers are located at $(y_{j-1/2}, z_{i-1/2})$. In (8) and at horizontal cell interfaces, V and $\partial_z V/\eta$ are continuous, while at vertical interface centers, V and $\partial_y V/\eta$ are continuous, commensurate with the discussion of the last section.

Integration of (7) over a computational cell, with application of the divergence theorem to transform the volume integral to a surface type, leads to

$$\int_{z_{i-1}}^{z_i} \mathrm{d}z \left[\partial_y V/\eta\right]_{y_{j-1}}^{y_j} + \int_{y_{j-1}}^{y_j} \mathrm{d}y \left[\partial_z V/\eta\right]_{z_{i-1}}^{z_i} - \int_{z_{i-1}}^{z_i}\int_{y_{j-1}}^{y_j} \mathrm{d}z\, \mathrm{d}y \gamma V = 0 \tag{9}$$

The use of (8) in (9) yields the matrix equation

$$\mathbf{Av} = \mathbf{f} \tag{10}$$

For this 2-D problem, **A** is a five-banded matrix whose elements are

$$A_{ij}^1 = \alpha_{ij} \frac{2\,\Delta y_j}{\eta_{ij}\,\Delta z_i + \eta_{i-1,j}\,\Delta z_{i-1}}$$

$$A_{ij}^2 = \beta_{ij} \frac{2\,\Delta z_i}{\eta_{i,j-1}\,\Delta y_{j-1} + \eta_{ij}\,\Delta y_j}$$

$$A_{ij}^4 = \beta_{ij} \frac{2\,\Delta z_i}{\eta_{i,j+1}\,\Delta y_{j+1} + \eta_{ij}\,\Delta y_j}$$

$$A_{ij}^5 = \alpha_{ij} \frac{2\,\Delta y_j}{\eta_{i+1,j}\,\Delta z_{i+1} + \eta_{ij}\,\Delta z_i}$$

$$A_{ij}^3 = -\left(A_{ij}^1 + A_{ij}^2 + A_{ij}^4 + A_{ij}^5\right) - \gamma_{ij}\,\Delta z_i\,\Delta y_j \tag{11}$$

and

$$\alpha_{ij} = 1 - \frac{\gamma_{ij}\eta_{ij}(\Delta z_i)^2}{8}$$

$$\beta_{ij} = 1 - \frac{\gamma_{ij}\eta_{ij}(\Delta y_j)^2}{8}$$

The components of **A** must be modified appropriately at the edges of the mesh to meet the boundary conditions. The vector **f** also incorporates boundary values.

The matrix eqn. (10) is similar to the usual form obtained in any fixed mesh finite difference (FD) or FE numerical approximation. An adaptive mesh approach requires additional equations for the movement of (y_j, z_i). From the calculus of variations (Clegg, 1968), it can be shown that the solution of (7) (with boundary conditions) provides a minimum for the Lagrangian form

$$L = \int \mathrm{d}y \int \mathrm{d}z H(V, \partial_y V, \partial_z V)$$

$$= \tfrac{1}{2}\mathrm{Re}\left\{ \int \mathrm{d}y \int \mathrm{d}z \left[(\partial_y V)^2/\eta + (\partial_z V)^2/\eta + \gamma V^2\right] + \sum_{l=1}^{2} \int \mathrm{d}y (-1)^l \left(\alpha^l V^2 - 2\beta^l V\right) + \sum_{l=3}^{4} \int \mathrm{d}z (-1)^l \left(\alpha^l V^2 - 2\beta^l V\right) \right\} \tag{12}$$

This means that (7) is the Euler equation obtained from the variation of L with respect to V that minimizes (12). For the FE formulation, the discrete form of (12) becomes

$$L_{FE} = \tfrac{1}{2}\mathrm{Re}\left\{ \sum_{i=1}^{N}\sum_{j=1}^{M} \left[\frac{1}{4\eta_{ij}} \sum_{n=1}^{4} \left[\left(a_{ij}^n\right)^2 + \left(b_{ij}^n\right)^2\right] + \gamma_{ij} V_{ij}^2 + \gamma_{ij} \left(\frac{V_{ij}}{2}\left(a_{ij}^2 - a_{ij}^1\right)\Delta y_j + \frac{V_{ij}}{2}\left(b_{ij}^1 - b_{ij}^3\right)\Delta z_i + \frac{1}{12}\left[\left(a_{ij}^2\right)^2 + \left(a_{ij}^1\right)^2\right](\Delta y_j)^2 + \frac{1}{12}\left[\left(b_{ij}^3\right)^2 + \left(b_{ij}^1\right)^2\right](\Delta z_i)^2 - \frac{1}{32}\left(a_{ij}^1 - a_{ij}^2\right)\left(b_{ij}^1 - b_{ij}^3\right)\Delta y_j\,\Delta z_i \right) \right] \times \Delta y_j\,\Delta z_i \right\} \tag{13}$$

The first variation of (13) with respect to the V_{ij} will give the FE set (10)–(11). To get an MFE formulation, additional equations for y_j and z_i will be obtained in a similar manner.

There are several complications that can arise when the FE mesh is allowed to move adaptively. The most prominent of these is the obvious requirement that two nodes not be allowed to occupy the same location or pass each other. To eliminate these problems, note that arbitrary functions in y and z can be added to the Lagrangian

in (13) without affecting the variation with respect to V which gives (10). This results from the form of the Euler equations for the minimization of (12). The particular form of these functions can be chosen to control the movement of the nodes y_j and z_i. Following Miller (1981), (13) is modified to give

$$\bar{L} = L_{FE} + \sum_{i=1}^{N} \left(\epsilon \, \Delta z_i - \frac{c_1}{\Delta z_i} \right)^2 + \sum_{j=1}^{M} \left(\epsilon \, \Delta y_j - \frac{c_2}{\Delta y_j} \right)^2 \tag{14}$$

where ϵ, c_1, and c_2 are constants. The additional entries in (14) are penalty or regularization ones which ensure a stable solution by controlling the allowed node spacing. The terms involving ϵ are frictional, and produce smooth rather than abrupt movement of the nodes, especially when the solution changes very slowly from element to element. The terms involving c_1 and c_2 are internodal repulsive ones which prevent two nodes from occupying the same position. The constants ϵ, c_1, and c_2 are chosen empirically to avoid these problems; their values are not critical. Miller (1981) discusses the importance of regularization in MFE. The penalty function used for node control is not unique; a variety of other constraints could be used as long as they are physically reasonable.

The solution $\{V_{ij}, y_j, z_i\}$ which minimizes (14) is obtained from the first variations of the Lagrangian with respect to the variables

$$\partial_V \mathrm{L} = \mathbf{Av} - \mathbf{f} = 0 \tag{15}$$

$$\partial_y \mathrm{L} = \epsilon^2 \mathbf{Ty} + \mathbf{Q}_1(V, y, z) = 0 \tag{16}$$

$$\partial_z \mathrm{L} = \epsilon^2 \mathbf{Tz} + \mathbf{Q}_2(V, y, z) = 0 \tag{17}$$

where $\mathbf{T}$ is tridiagonal with -2 on the main diagonal and 1 in the off-diagonal locations, and $\mathbf{y}$ and $\mathbf{z}$ are vectors of node co-ordinates. In (15)–(17), the dependence on $\mathbf{y}$ and $\mathbf{z}$ is nonlinear in the $\mathbf{A}$ matrix and the $\mathbf{Q}_1$ and $\mathbf{Q}_2$ vectors because of the regularization terms in (14).

To solve the MFE equations (15)–(17), an initial mesh must be specified; a simple, evenly spaced type within regions of constant conductivity generally is sufficient. An initial solution for $\mathbf{v}$, obtained by solving (15) alone, will not usually satisfy (16) and (17), so the set is linearized and a Newton iterative solution is found. This typically requires three to five iterations. In practice, some simplifications can be made in the numerical solution of (15)–(17). Rather than solving all three sets of equations simultaneously, (15) can be solved for the current values of $\{V_{ij}, y_j, z_i\}$, then (16) and (17) can be treated separately, neglecting linearization of the nonlinear terms $\mathbf{Q}_1$ and $\mathbf{Q}_2$, to modify the node locations. This means that only tridiagonal equations are solved for $\mathbf{y}$ and $\mathbf{z}$ at each iteration. This approximate form works well for the sample problems discussed later.

The FE solution of (4)–(7) requires the specification of σ on a finite size grid $z_1 \leqslant z \leqslant z_2$, $y_1 \leq y \leq y_2$. The conductive Earth is assumed to lie in the region $0 \leq z \leq z_2$, while the half space $z < 0$ is nonconducting air. Boundary conditions must be specified on the outer limits of the mesh at z_1, z_2, y_1, and y_2. At the upper boundary z_1, the zero wavenumber nature of the MT source fields leads to the requirement of a constant horizontal magnetic field. For the TM mode, (5) shows that B_x is constant in a nonconductor, and z_1 may be chosen as the interface $z = 0$. For the TE mode, z_1 must be negative and sufficiently large that secondary fields induced by lateral changes in media properties are small, a distance typically of order the horizontal model dimension. The bottom boundary z_2 must be deep enough that the principal fields are negligible, and either one-dimensionality or a perfect conductor may be assumed below $z = z_2$. A variety of conditions for the model edges are in use. Rodi (1976) discussed periodic ($\partial_y V = 0$) and approximate conditions for use at y_1 and y_2. The latter involve an implicit assumption of one-dimensionality outside the mesh. For a lucid discussion of these points, see Rodi (1976).

The Maxwell eqn. (1) is a condition that is implicitly satisfied by the forms in Section 3, but that may not be explicitly met by a numerical solution owing to discretization and roundoff. For a more generalized finite element problem, common vector identities like $\nabla \cdot \nabla \times \mathbf{A} = 0$ and $\nabla \times \nabla \mathrm{U} = 0$ must hold for the FE solution, although this is not necessarily implicit in the formulation. Any numerical solution of the Maxwell equations

should be forced to satisfy as many of these types of constraints and continuity conditions as possible to ensure an accurate simulation. This generally requires FE representations higher than linear. In practice, a decision is made, explicitly or implicitly, to favor some of these constraints over others to avoid the added complexity of higher-order approximations. Neglect of any of these conditions can allow spurious numerical modes to appear, although they may be of no harm or may be damped by other physical processes included in the model equations. For the 2-D MT problem, the condition (1) and the vector identity $\nabla \cdot \nabla V = 0$ lead to the requirement that $\partial^2_{yz} V = \partial^2_{zy} V$, a condition that holds for (sufficiently differentiable) continuous variables but may not for a given FE formulation.

4. Efficient matrix solutions

A given FE scheme can also be improved through minimization of the usage of computer time and memory by taking advantage of the inherent structure of the FE equations. Both FD and FE discretizations lead to matrix equations of the form $\mathbf{Av} = \mathbf{b}$, where $\mathbf{A}$ is sparse (i.e., only a small fraction of its elements are nonzero), and (usually) symmetric and banded. The computational focus is then placed on optimizing a factorization of $\mathbf{A}$ to reduce the cost of solving the equations (Behie and Forsyth, 1984; Zyvoloski, 1986). A considerable improvement over conventional Gaussian elimination or LU decomposition can be achieved. For background on standard numerical methods for solving matrix problems, see Golub and Van Loan (1983).

The class of matrix methods known as incomplete factorization (ILU) has become quite popular for FD and FE calculations in many disciplines. ILU is an iterative procedure in which only one or (at most) a few Gaussian elimination steps are taken per iteration. Figure 1 illustrates the difference between the ordinary methods and ILU. In Gaussian elimination on a banded matrix, most of the entries between the original bands will be occupied at some time in the solution process by a computed, intermediate result even though the entry value originally was zero. With ILU, fewer locations are filled, or a particular entry is re-computed fewer times, leading both to faster execution and to a smaller memory storage requirement. Some new variants have been developed to improve on ILU schemes. For example, variable ILU (VILU) changes the number of Gaussian elimination steps per iteration in different parts of the matrix depending on local conditions and the structure of the matrix problem. Behie and Forsyth (1984) and Zyvoloski (1986) discussed ILU and VILU for solving FE and FD matrices. Details of the ILU or VILU scheme depend critically on the form of the equations being solved and on the discretization used to parameterize the problem. A real advantage of this approach is its relative insensitivity to the dimensionality of a simulation because of the partial fill-in. This should become very significant in 3-D applications.

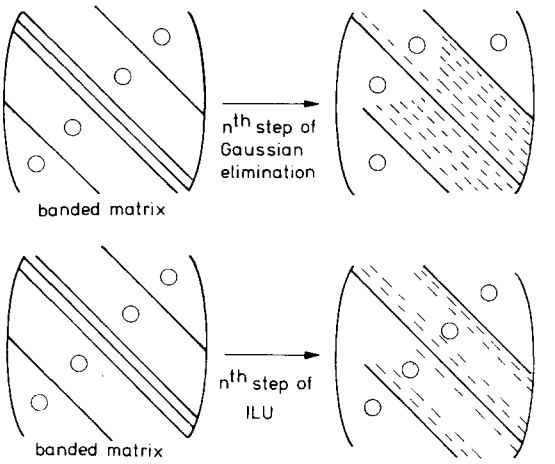

Fig. 1. Sketch illustrating the differences between ordinary Gaussian elimination and an ILU method on a banded matrix. The solid diagonal lines indicate the matrix bands, which contain nonzero matrix elements, while the large zeroes indicate regions where the matrix contains no entry. The top part of the figure shows that Gaussian elimination fills most of the empty locations with an intermediate result during computation. The bottom part of the figure indicates that ILU addresses many fewer such elements in the matrix.

Another enhancement in solving matrix equations arises from changing the order in which the nodes are processed. Red/black partitioning re-

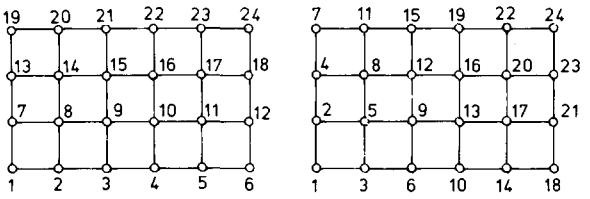

Fig. 2. A comparison of a typical ordering for finite element matrices with red/black ordering: (a) shows a standard ordering, in which the node addresses are set up in a straightforward manner; (b) shows the red/black ordering, in which the node addresses have been redefined to facilitate reduction of the matrix.

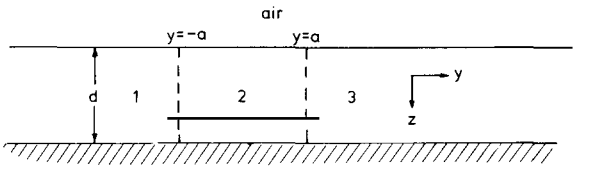

Fig. 3. The geometry of the control model of Weaver et al. (1985, 1986). The conductive structure consists of three regions of different conductivity and uniform thickness, d, separated at the interfaces $y = -a$ and $y = a$. The conducting media are overlain by nonconducting air and underlain by a perfect conductor.

orders the nodes into red types, which have no red nearest neighbors, and black types, which constitute the remainder. The red terms are placed at the top of the matrix, and their associated equations can be removed by simple matrix transformations. Only the black node linear system has to be solved by ILU. This results in a reduction in the size of the problem by up to a factor of two, depending on the discretization used. Wolfe and Zyvoloski (1987) discuss a new partitioning, red/black squared, which involves two orderings, yielding a reduction in the size of the problem by up to a factor of three. Figure 2 compares a typical ordering for a FD or FE discretization with a red/black ordering. The increased computer time required to sort the matrix must be balanced against the savings in time from factorization; this will yield a substantial improvement for large problems.

The use of acceleration methods can also increase the speed of matrix computations. At each iteration in the ILU method, an estimate can be made of the direction and relative magnitude that the next correction to each dependent variable

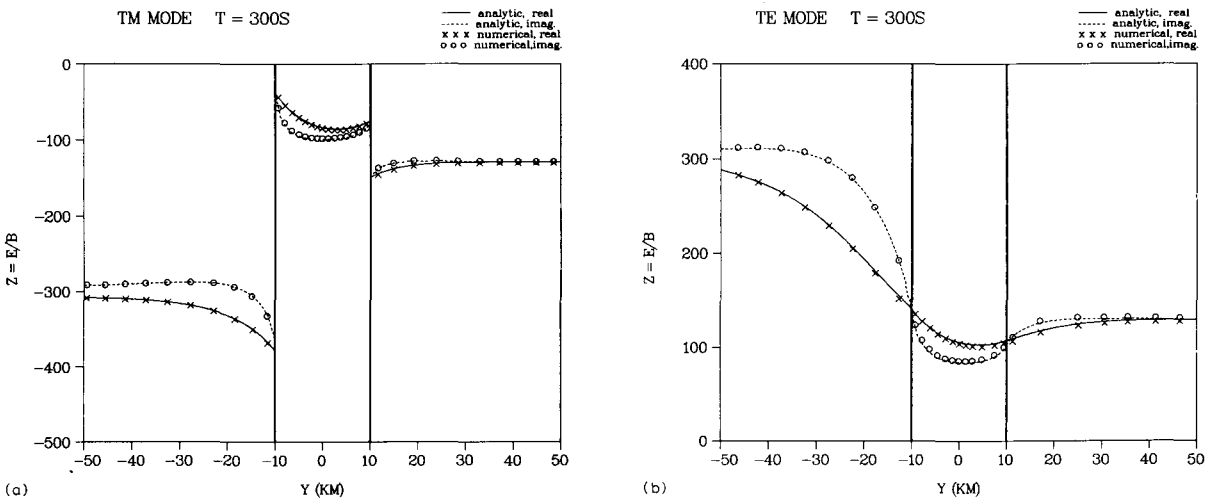

Fig. 4. Comparison of the analytic solutions of Weaver et al. (1985, 1986) for the (a) TM and (b) TE mode response functions with the MFE numerical results at a period of 300 s at the Earth's surface. The solid and dashed lines are the real and imaginary parts of the analytic E/B response function parameterized by horizontal distance, y; the interfaces separating the conductive regions are at -10 and 10 km and are delineated by the heavy vertical lines. The discrete symbols show the numerical results, with Xs for the real and circles for the imaginary parts.

should have to minimize the current matrix equation squared residuals. For symmetric matrices, the procedure is a conjugate gradient scheme with a carefully chosen step-size (Kershaw, 1978). For asymmetric matrices, the matrix equation residual is still minimized, but an additional orthogonalization step is required which transforms the matrix to its principal axes before determining the direction and magnitude of the optimal increment for the dependent variable vector. A popular procedure for asymmetric matrices is the ORTHOMIN method of Vinsome (1976). This also controls the condition number of the matrix.

Finally, vectorization on a modern supercomputer can dramatically improve computational efficiency. A Cray-class supercomputer derives its enhanced performance both by the use of significantly faster hardware and by implementing a number of new principles. The first of these is the vector instruction, in which a single machine instruction allows data vectors (as opposed to single elements) to be processed. The Cray allows vectors of 64 words to be treated in this way. Cray-class hardware also implements pipelining, in which a single operation is split into smaller pieces and separate parts of the machine are allocated to each. This performs much like an assembly line, so that independent parts of the hardware operate simultaneously on different parts of the data and pass the result on to the next station. A result can be delivered at each machine clock cycle using pipelining. These principles allow dramatic improvements in machine performance to be achieved, with peak execution rates in excess of 100 million floating point operations per second. Matrix calculations are particularly well-suited to vector machines, and the execution time can be nearly independent of the size of the problem. Dongarra et al. (1984) discuss the principles of vector pipeline computers and their use for linear algebra computations.

5. Validation of the MFE code

The current version of the magnetotelluric MFE code, named MTAM2D, has been validated by comparison to the standard analytic control models for the TM and TE modes developed by Weaver et al. (1985, 1986). Figure 3 displays the geometry of their test case. A conductive region of constant thickness, d, overlies a perfect conductor, and

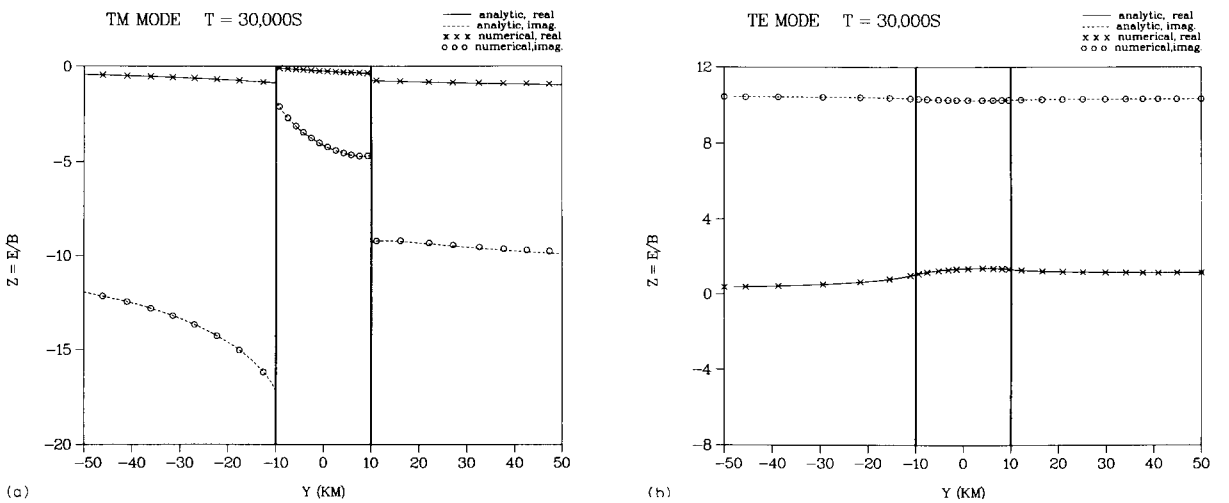

Fig. 5. Comparison of the analytic solutions of Weaver et al. (1985, 1986) for the (a) TM and (b) TE mode response functions with the MFE numerical results at a period of 30000 s at the Earth's surface. The solid and dashed lines are the real and imaginary parts of the analytic E/B response function parameterized by horizontal distance, y; the interfaces separating the conductive regions are at -10 and 10 km and are delineated by the heavy vertical lines. The discrete symbols show the numerical results, with Xs for the real and circles for the imaginary parts.

consists of three distinct zones with different conductivities $\sigma_1(y < -a)$, $\sigma_2(-a \leq y \leq a)$, and $\sigma_3(y > a)$. For this comparison, the variables have been chosen as follows

$a = 10$ km

$d = 50$ km

$\sigma_1 = 0.1$ S m^{-1}

$\sigma_2 = 1.0$ S m^{-1}

$\sigma_3 = 0.5$ S m^{-1}

Solutions for two periods T of 300 and 30 000 s for both modes were computed.

Figures 4 and 5 compare the analytic and numerical results for the ratio E/B as a function of y at the Earth's surface $z = 0$ for the TM and TE modes at the two periods. The size of the initial FE mesh (i.e., the number of nodes) was adjusted empirically to the minimum required to achieve acceptable accuracy for each case. The initial mesh for the TM mode 300 s numerical solution consisted of 30 uniformly sized zones in the vertical direction and 60 zones in the horizontal—30, 15, and 15 uniformly spaced zones in the three conductive regions, respectively. At 30 000 s period, the initial mesh contained only 20 zones vertically and 45 horizontally—20, 10, and 15 zones in the three conductive regions. For the TE case at the shorter period, the vertical zoning was modified to include 12 sections in air ($z < 0$) and 20 within the Earth ($z > 0$), while the horizontal zoning included 49 uniformly spaced regions—25, 12, and 12 zones in the three conductive regions. At 30 000 s, the TE mesh was reduced to 10 and

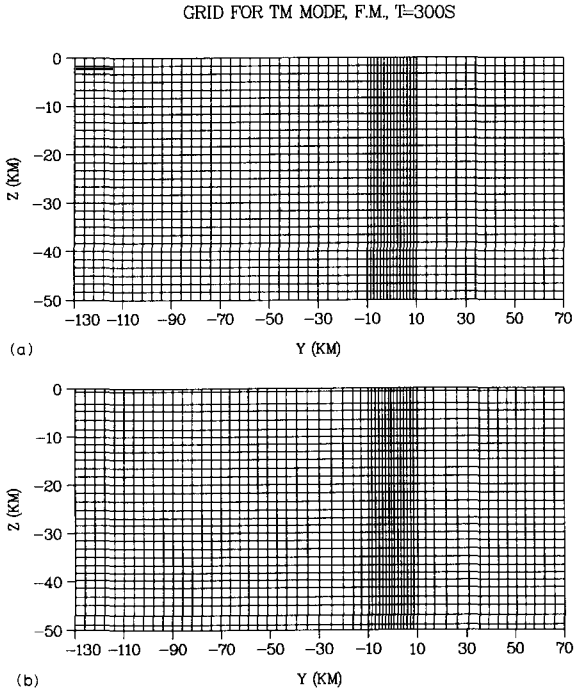

Fig. 6. The (a) initial and (b) final meshes for the MFE solution of Fig. 4a for the TM mode at 300 s period. The initial mesh was uniform, with 30 zones in the vertical and 60 zones in the horizontal (30, 15, and 15 in the three conductive regions). The final mesh has been adaptively modified to concentrate the nodes where the electromagnetic field is changing most rapidly, especially the boundaries between conductive regions and the Earth–atmosphere contact at $z = 0$.

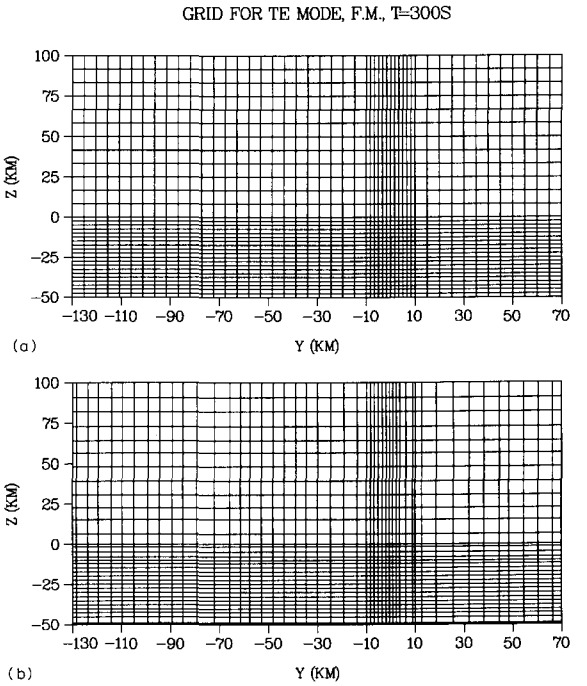

Fig. 7. The (a) initial and (b) final meshes for the MFE solution of Fig. 4b for the TE mode at 300 s period. The initial mesh was uniform, with 32 zones in the vertical (12 in air and 20 within the model Earth), and 49 zones in the horizontal (25, 12, and 12 zones in the three conductive regions). The final mesh has been adaptively modified to concentrate the nodes where the electromagnetic field is changing most rapidly, especially the boundaries between conductive regions and the Earth–atmosphere contact at $z = 0$.

20 vertical zones in air and Earth, and 45 uniform horizontal zones—20, 10, and 15 sections in the three regions. The side boundaries were located at $y = -130$ and $y = 70$ km for all of the models, sufficiently far from the conductive transitions to not affect the solution, and the horizontal derivatives of the fields were taken to vanish at those points (periodic boundary conditions). At the bottom of the model for the TM mode, $\partial_z B_x$ was set to zero, while $B_x = 1$ at the surface $z = 0$. As for the TE mode, E_x was set to zero at the bottom of the model, and $\partial_z E_x$ was set to $i\omega\mu$ at $z = z_1$. The regularization parameters in (14) were set as $\epsilon = 10^{-5}$, $c_1 = c_2 = 5 \times 10^{-2}$ for the TM mode and $\epsilon = 10^{-8}$, $c_1 = c_2 = 5 \times 10^{-5}$ for the TE mode. The quantity being minimized in (14) takes on considerably different values for the TE and TM mode cases, varying over a range of several hundred. Accordingly, the values of the penalty term constants ϵ, c_1, and c_2 must be changed to keep the corresponding terms in (14) small relative to the L_{FE} term. Variations of a factor of 10 about the specified values do not affect the result appreciably. Computer run times for all calculations were < 2 s on a Cray X-MP.

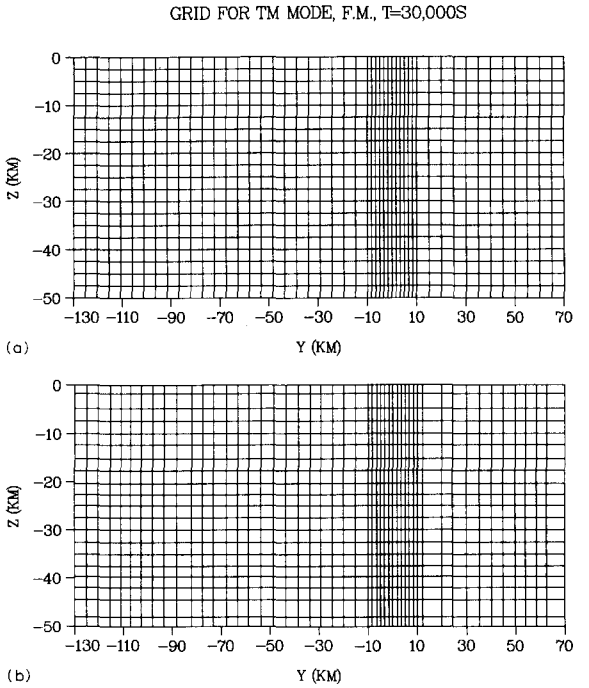

Fig. 8. The (a) initial and (b) final meshes for the MFE solution of Fig. 5a for the TM mode at 30000 s period. The initial mesh was uniform, with 20 zones in the vertical and 45 in the horizontal (20, 10, and 15 in the three conductive regions).

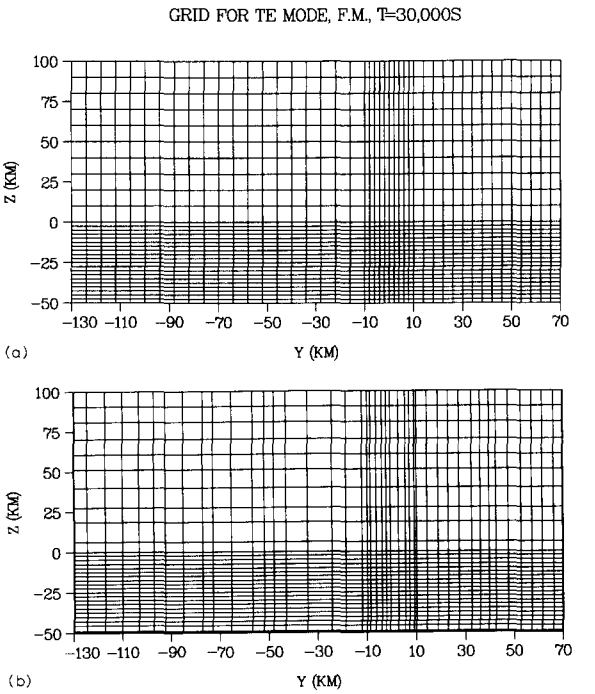

Fig. 9. The (a) initial and (b) final meshes for the MFE solution of Fig. 5b for the TE mode at 30000 s period. The initial mesh was uniform, with 30 zones in the vertical (10 and 20 in air and Earth) and 45 zones in the horizontal (20, 10 and 15 in the three regions).

The adaptive mesh scheme moved the nodes so that the Lagrangian in (14) was minimized. This also resulted in a smaller value for the non-penalized Lagrangian in (12). Generally, no further decrease occurs in the Lagrangian values after a few iterations. The initial and final meshes are shown in Figs. 6–9, corresponding to the models in Figs. 4 and 5. The nodes are shifted near the vertical boundaries at $y = -a$ and $y = a$, near the surface at $z = 0$, and in regions where the electromagnetic fields are changing rapidly. As would be expected, the zones near the boundaries and at the interior interfaces become smaller so that derivatives of the fields can be resolved more precisely. In the interior region between $y = -a$ and $y = a$,

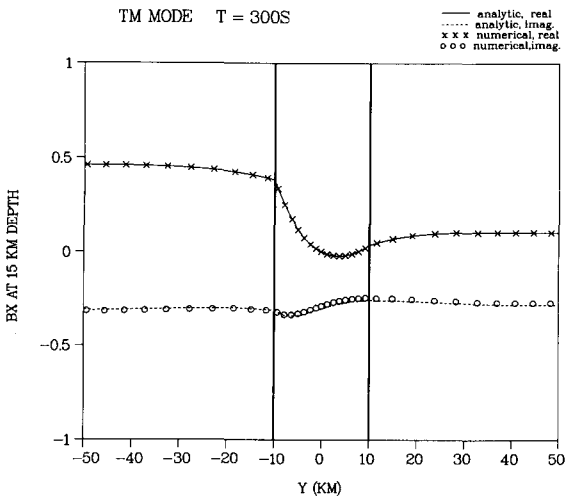

Fig. 10. The magnetic field component B_x for the TM mode at 300 s period and a depth of 15 km inside the Earth. Note the points at which the fields are changing most rapidly and compare with Fig. 4.

the zoning changes in an asymmetrical fashion. For example, in the 300 s case in Fig. 4, the zones have shifted to the centre between $y = -10$ and $y = 10$ km. The reason for this becomes apparent after inspection of Fig. 10, which shows the field component B_x against the horizontal co-ordinate y inside the model Earth at $z = 15$ km. That curve is fairly steep in the left part of the middle conductive region, but flattens out on the right-hand section. Curvature is greatest around $z = 0$. The zoning will tend to reflect the structure of the electromagnetic field component that is actually solved for, not the response function that is obtained from the fields. This accounts for the apparent discrepancies in node locations between Figs. 6–9 and the shapes of the response function curves shown in Figs. 4 and 5. The adaptive meshes are sometimes not as smooth as one would expect, as in Fig. 9. This is owing to choosing poor values for the constants in (14). If regularization parameters are too small, the system will tend to become ill-conditioned. Practice with the model is required to find the optimal range of regularization parameter values.

In retrospect, the mesh changes obtained for the test cases are significant but not dramatic. There are several factors acting to cause this. For one, the analytic solutions involve only variations in conductivity in the $\hat{y}$ direction, and the changes in conductivity between the regions are not large. In addition, this first version of the code, in the interest of simplicity, required a specified number of nodes in each region. When this restriction is relaxed to simply require specification of the number of nodes for the entire mesh, greater mesh deformation will be observed. Another factor is the nature of the numerical mesh. Because the mesh uses rectangular elements with square corners in the current version of the MFE code, all points on a vertical or horizontal grid line are constrained to move simultaneously. The mesh is actually responding to the average gradient of the solution along a y or z grid line. This restriction results in less node movement than is desirable. The rectangular elements used here will be replaced with triangular types in the next version of the code, improving its ability to handle non-horizontal interfaces. This will also allow the nodes to move individually and improve the adaptability of the result. Nevertheless, the principle of MFE is well-illustrated by the examples in Figs. 4 and 5. The advantages of an adaptive mesh in minimizing mesh design problems and maximizing the resolution for a given size mesh are obvious, although careful design of the mesh using a fixed mesh model would probably give answers that are just as good. Adaptive procedures should reduce the human time involved in solving forward problems, and will be of definite advantage for inversion when the locations of conductivity boundaries may not be known a priori.

References

Behie, G.A. and Forsyth, P.A., 1984. Incomplete factorization methods for fully implicit simulation of enhanced oil recovery. SIAM J. Sci. Stat. Comp., 5: 543–561.

Clegg, J.C., 1968. Calculus of Variations. Oliver and Boyd, Edinburgh.

Coggon, J.H., 1971. Electromagnetic and electrical modelling by the finite element method. Geophysics, 36: 132–155.

Dongarra, J.J., Gustavson, F.G. and Karp, A., 1984. Implementing linear algebra algorithms for dense matrices on a vector pipeline machine. SIAM Rev., 26: 91–112.

Dukowicz, J.K., 1984. A simplified adaptive mesh technique derived from the moving finite element method. J. Comp. Phys., 56: 324–342.

Gelinas, R.J., Doss, S.K. and Miller, K., 1981. The moving finite element method: applications to general partial differential equations with multiple large gradients. J. Comp. Phys., 40: 202–249.

Golub, G.H. and Van Loan, C.F., 1983. Matrix Computations. Johns Hopkins University Press, Baltimore, 475 pp.

Kershaw, D.S., 1978. The incomplete Cholesky conjugate gradient method for the iterative solution of systems of linear equations. J. Comp. Phys., 26: 43–65.

Lee, K.H. and Morrison, H.F., 1985. A numerical solution for the electromagnetic scattering by a two-dimensional inhomogeneity. Geophysics, 50: 466–472.

Miller, K., 1981. Moving finite elements—II. SIAM J. Num. Anal., 18: 1033–1057.

Miller, K. and Miller, R.N., 1981. Moving finite elements—I. SIAM J. Num. Anal., 18: 1019–1032.

Pridmore, D.F., Hohmann, G.W., Ward, S.H. and Sill, W.R., 1981. An investigation of finite-element modelling for electrical and electromagnetic data in three dimensions. Geophysics, 46: 1009–1024.

Rodi, W.L., 1976. A technique for improving the accuracy of finite element solutions for magnetotelluric data. Geophys. J. R. Astron. Soc., 44: 483–506.

Vinsome, P.K.W., 1976. ORTHOMIN: an iterative method for solving sparse sets of simultaneous linear equations. Fourth SPE Symp. on Num. Sim. of Reservoir Perf., Los Angeles, paper SPE5729.

Wannamaker, P.E., Stodt, J.A. and Rijo, L., 1985. PW2D—finite element program for solution of magnetotelluric responses of two-dimensional earth resistivity structure: program documentation. University of Utah Research Institute Report ESL-158, 71 pp.

Wannamaker, P.E., Stodt, J.A. and Rijo, L., 1987. A stable finite element solution for two-dimensional magnetotelluric modelling. Geophys. J. R. Astron. Soc., 88: 277–296.

Weaver, J.T., Le Quang, B.V. and Fischer, G., 1985. A comparison of analytic and numerical results for a two-dimensional control model in electromagnetic induction—I. B-polarization calculations. Geophys. J. R. Astron. Soc., 82: 263–277.

Weaver, J.T., Le Quang, B.V. and Fischer, G., 1986. A comparison of analytic and numerical results for a two-dimensional control model in electromagnetic induction—II. E-polarization calculations. Geophys. J. R. Astron. Soc., 87: 917–948.

Wolfe, J. and Zyvoloski, G., 1987. Comparison of reordering schemes in incomplete factorization methods. Los Alamos National Laboratory Report LA-UR-86-2527.

Zyvoloski, G., 1986. Incomplete factorization for finite element methods. Int. J. Num. Meth. Eng., 23: 1101–1109.